

# Estimating Metric Poses of Dynamic Objects Using Monocular Visual-Inertial Fusion

Kejie Qiu\*, Tong Qin\*, Hongwen Xie<sup>†</sup>, and Shaojie Shen\*

**Abstract**—A monocular 3D object tracking system generally has only up-to-scale pose estimation results without any prior knowledge of the tracked object. In this paper, we propose a novel idea to recover the metric scale of an arbitrary dynamic object by optimizing the trajectory of the objects in the world frame, without motion assumptions. By introducing an additional constraint in the time domain, our monocular visual-inertial tracking system can obtain continuous six degree of freedom (6-DoF) pose estimation without scale ambiguity. Our method requires neither fixed multi-camera nor depth sensor settings for scale observability, instead, the IMU inside the monocular sensing suite provides scale information for both camera itself and the tracked object. We build the proposed system on top of our monocular visual-inertial system (VINS) to obtain accurate state estimation of the monocular camera in the world frame. The whole system consists of a 2D object tracker, an object region-based visual bundle adjustment (BA), VINS and a correlation analysis-based metric scale estimator. Experimental comparisons with ground truth demonstrate the tracking accuracy of our 3D tracking performance while a mobile augmented reality (AR) demo shows the feasibility of potential applications.

## I. INTRODUCTION

A complete robotic perception system consists of robust state estimation (localization), static environment mapping and dynamic objects tracking, through the use of multiple onboard sensors. Among these diverse sensing options, we are particularly interested in the minimal sensor suite that consists of only one camera and an IMU, due to its ultra light-weight and low-cost. Equipped with state estimation and mapping that comprise a simultaneous localization and mapping (SLAM) system, an agent like a quadrotor can execute autonomous navigation within an unknown but static environment [1]. However, for a complete perception system, dynamic objects in the real world also have to be considered seriously. Previously, dynamic objects are often regarded as outliers in a SLAM system, and the main consideration is how to make the autonomous system robust against these outliers. In other words, static environment is a basic assumption. Nevertheless, a better way is to actively track the dynamic objects regarding 6-DoF pose estimation, thus completing the whole perception system as shown in Fig. 1. And a lot of benefits will follow if the specific position

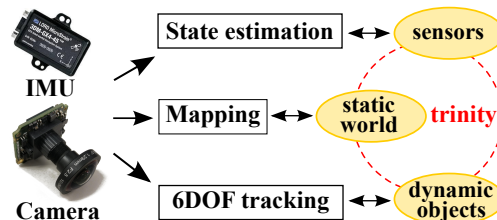


Fig. 1: The complete perception system based on monocular visual-inertial sensing.

and orientation of the dynamic object are known. More robust state estimation, active obstacle avoidance, and path planning, manipulation of the objects, even augmented reality effect on the moving objects can become possible.

Actually, although promising results on state estimate and static environment mapping have been achieved using monocular visual-inertial fusion [2], [1], six degree of freedom (6-DoF) metric tracking of dynamic objects remains a significant challenge. It is obvious that the metric scale or the real depth value of dynamic objects is of significant importance for various real-time applications. While the primary difficulty comes from the fact that the metric scale is not directly observable from only one camera. To handle this, one common solution is to utilize multiple fixed cameras such that the triangulation constraint is still valid even the objects are moving. Motion capture system such as OptiTrack<sup>1</sup> and Vicon<sup>2</sup> have been a mature tracking system for moderately sized application scenarios but the tracked objects have to be attached with reflective markers.

On the other hand, single sensor-based methods using an RGBD sensor [3] or a stereo camera [4] relax the multi-sensor condition at the cost of limited sensing distance. Consequently, these methods can only handle small-scale application situations such as vision-based object manipulation. We regard the camera motion and object motion as two isolated signals and recover the metric object motion from the perspective of signal processing, say, signal correlation analysis. This process is like the signal decomposition problem discussed in the telecommunication community. Thus, we propose to estimate the metric scale by analyzing the temporally statistical relationship between the camera motion and the recovered object motion.

The rest of the paper is structured as follows. Section II introduces relevant work on 6-DoF object pose estimation and fundamental work that our system relies on. In sec-

\*Kejie Qiu, Tong Qin and Shaojie Shen are with the Department of Electronic and Computer Engineering, Hong Kong University of Science and Technology, Hong Kong, China. kqiu@connect.ust.hk, tqin@connect.ust.hk, eeshaojie@ust.hk.

<sup>†</sup>Hongwen Xie is from Pattern Recognition Center of WeChat, Tencent Inc, Beijing, China. hongwenxie@tencent.com.

This work was supported by the WeChat-HKUST Joint Laboratory on Artificial Intelligence Technology (WHAT LAB).

<sup>1</sup><http://optitrack.com/>

<sup>2</sup><http://www.vicon.com/>

tion III, our system structure and major frame relationships are illustrated briefly. Section IV describes how the objective functions are formulated and solved for up-to-scale 3D tracker and metric scale estimation. Section V gives the experimental results with comparison against ground truth. Conclusion and directions for future work are presented in Section VI.

## II. RELATED WORK

Estimating the 6-DoF pose of a dynamic object using multiple fixed cameras is a well-studied formulation. Besides the commercial active-tracking system with specialized markers, passive-tracking systems for sports scenes analyzing and traffic surveillance were also proposed since the targets are usually non-cooperative in these cases. A UAV trajectory estimation system using flight dynamics as a prior was proposed based on fixed ground cameras, assuming that all the camera videos are synchronized [5]. [6] proposed a spatiotemporal Bundle Adjustment framework to simultaneously estimate the temporal alignment between cameras. However, all of these methods are limited by the fixed-camera setting.

Oppositely, few methods adopt a monocular camera framework to recover the whole 6-DoF pose of dynamic objects, since the tracking results may lack metric scale unless the tracked target is studied or modeled carefully in advance. However, solving this problem only using single camera has attracted even more attention thanks to its ultra lightweight, strong adaption, and synchronization-free features compared to the fixed multi-camera setting. Model-based tracking is one branch of monocular-based methods. Given a set of known 2D-to-3D correspondences, the relative pose can easily be solved by using Perspective-n-Point (PnP) [7] or view alignment using edge features [8], [9]. For instance, ARUCO tag [10] made use of pre-designed tags as the known 3D information to mark tracked targets, and calculate the camera pose in terms of the tags. Instead of using pre-designed landmarks, discriminative feature points such as BRISK [11] are also practical for 2D-to-3D matching. In addition to sparse point features, dense method [12] and edge-based method [13] are good alternatives for textureless object tracking. All the methods work well as long as the 3D model of the tracked object was carefully modeled in advance. Another significant branch is learning-based tracking [14], Georgios Pavlakos et al. proposed an efficient convolutional network to first locate reliable pre-defined semantic keypoints and then estimate the 6-DoF pose with only a monocular camera [15]. However, a faked scenario can destroy learning-based methods easily especially in AR applications. For example, a real car and a car model can fool learning-based methods for lack of metric scale measurement.

In order to estimate the metric object scale, the camera pose has to be known in advance such that the object pose computed from the region-based BA can be projected from the camera frame to the world frame. And we make use of our visual-inertial system (VINS) for accurate and robust camera pose estimation in the world frame, interested readers are referred to our previous work on state estimation with

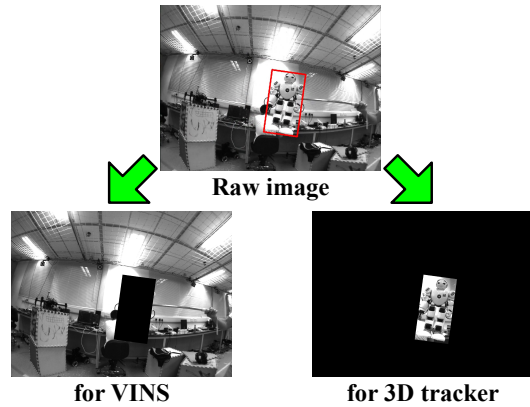


Fig. 2: 2D object tracking results with bounding boxes.

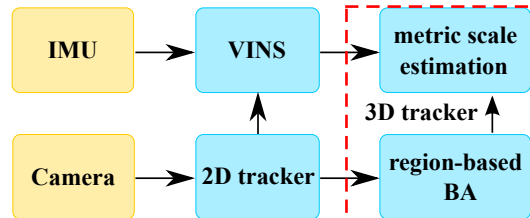


Fig. 3: Overall system structure.

visual-inertial fusion [16], [17]. Also, our method is designed to handle 6-DoF tracking of an arbitrary rigid object by using an object region-based visual bundle adjustment (BA) with online scale estimation. In order to obtain accurate object regions for region-based visual BA, a robust 2D tracker is needed. The 2D tracking problem has already been well discussed and lots of classic tracking methods such as CMT [18], STRUCK [19] are robust enough for most cases, resulting in sequential bounding boxes. Given accurate object areas on the sequentially images, a region-based BA could be used to get up-to-scale relative 6-DoF pose.

## III. SYSTEM OVERVIEW

The captured images are first processed by 2D object tracking, resulting in object regions represented by 2D bounding boxes as shown in Fig. 2. VINS [17] takes both IMU and masked images for tightly-coupled camera pose estimation in the world frame. Given consecutive image regions of the object, a region-based visual BA is running for up-to-scale object pose estimation. Finally, the camera pose in the world frame and the object pose in the camera frame are collected together for metric scale estimation. Once the metric scale estimation obtained, the metric object poses in the world frame is recovered. The overall system structure is shown in Fig. 3. The combination of the region-based BA and metric scale estimation is also called 3D tracker, while up-to-scale 3D tracker particularly refers to the region-based BA. In this paper, we assume that a 2D object detector is provided for 2D tracking initialization and focus on region-based visual bundle adjustment and online metric scale estimation.

The relationship between relevant frames is shown in Fig. 4, where  $(\cdot)^w$  is the world frame,  $(\cdot)^c$  the camera frame, and

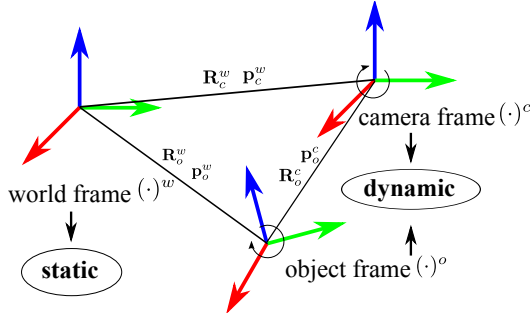


Fig. 4: Coordinate frames in the system.

$(\cdot)^o$  is the object frame. The IMU frame is ignored since it only constrains the metric scale of VINS.  $\mathbf{p}_y^x$  and  $\mathbf{R}_y^x$  are the 3D translation and rotation of frame  $(\cdot)^y$  respectively with respect to frame  $(\cdot)^x$ . The camera pose in the world provided by VINS is represented by  $\mathbf{R}_c^w$  and  $\mathbf{p}_c^w$ , and  $(\cdot)$  denotes the up-to-scale pose results. Thus  $\mathbf{R}_o^c$  and  $\bar{\mathbf{p}}_o^c$  together denotes the relative transformation of the object frame in terms of the camera frame provided by the region-based visual BA module. What the metric scale estimation module estimates is the scale ratio  $s$  that makes the up-to-scale position to scaled one ( $\mathbf{p}_o^c = s \cdot \bar{\mathbf{p}}_o^c$ ). In the end, we use  $\mathbf{R}_o^w$  and  $\mathbf{p}_o^w$  together to denote the global transformation from the world frame to the object frame. The detailed representation of the global object pose can be found in Section IV.

## IV. METHODOLOGY

### A. Up-to-scale 3D tracker

The 3D tracker we design is based on a region-based visual bundle adjustment, we construct a purely vision-based graph optimization for 3D pose tracking of general objects. In this way, any rigid objects with arbitrary shapes could be tracked since no assumption about the object shape is needed. Note that this bundle adjustment is performed with respect to the object frame, that is, the 3D tracker is to estimate the camera motion w.r.t the object frame, which is different from the visual BA defined in VINS with estimating the camera motion w.r.t the world frame. Since both camera frame and object frame are dynamic, either camera motion or object motion can cause the relative motion detected by the region-based visual BA. That is to say, the estimated motion of the 3D tracker is a compound motion coupled with two independent physical motions.

The full state of a sliding window with  $N$  image frames and  $M$  object features is defined as follows:

$$\begin{aligned} \mathcal{X} &= [\mathbf{x}_0, \mathbf{x}_1, \dots, \mathbf{x}_{N-1}, \mu_0, \mu_1, \dots, \mu_{M-1}] \\ \mathbf{x}_k &= [\bar{\mathbf{p}}_{o_k}^{c_k}, \mathbf{q}_{o_k}^{c_k}], k \in [0, N-1], \end{aligned} \quad (1)$$

where the  $k$ -th camera state consists of the up-to-scale position  $\bar{\mathbf{p}}_{o_k}^{c_k}$ , and orientation  $\mathbf{q}_{o_k}^{c_k}$  of camera frame  $c_k$  with respect to object frame  $o_k$ . 3D features are parameterized by their inverse depth  $\mu$  when first observed in camera frame. The bundle adjustment can be formulated as a nonlinear least-square problem,

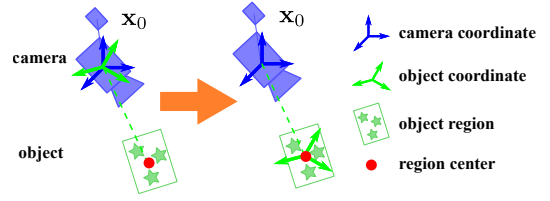


Fig. 5: Object coordinate initialization process.

$$\min_{\mathcal{X}} \sum_{(l,j) \in \mathcal{C}} \|\mathbf{r}_c(\hat{\mathbf{z}}_l^{c_j}, \mathcal{X})\|_2^2, \quad (2)$$

where  $\mathbf{r}_c(\hat{\mathbf{z}}_l^{c_j}, \mathcal{X})$  is the nonlinear residual function of visual measurements. The vector  $\mathbf{z}_l^{c_j}$  results from the procedure where the  $l$ th feature is projected to camera frame  $c_j$ . And the visual residual is defined as the sum of the reprojection error between the projected 3D features and the observed 2D features. Since this formulation takes the object regions of the captured images as input, the object is used as the reference frame for camera pose estimation. The front end of the region-based visual BA for feature association adopts the same corner features as that used in VINS, which could be replaced by other feature-based methods, such as edge-based and dense methods to handle featureless objects.

The direct optimization results are camera transformations in terms of the object frame, while what we need for 3D object tracking is the object pose in the camera frame. Thus, the object coordinate has to be located around the object itself, which is not guaranteed by a regular visual BA. To solve this problem, we further modify the initial poses by estimating the initial object pose in the camera frame. As shown in Fig. 5, we move the object coordinate from the initial position where the initial camera optical center locates to the object surface along the direction denoted by the 2D object region center, and normalize the object depth by scaling the object point cloud simultaneously. In fact, the object coordinate can be anywhere around the point cloud on the object, once it's determined in the initialization process, it will be continuously tracked in the bundle adjustment framework.

### B. Metric scale estimation

Before doing metric scale estimation, we already have accurate enough camera poses in the world frame, and up-to-scale object poses in the camera frame. Fundamentally, the metric scale of a tracked rigid object is unobservable based on a monocular camera. Consider an extreme case that the monocular sensor suite is always static when tracking the object, the IMU that involves scale information will have no contribution to the object scale recovery. However, the metric scale estimation problem becomes conditionally solvable if the camera motion and the object motion follow a specific condition, or scale observability condition. Since the intrinsic scale estimation could work with the region-based bundle to provide continuous metric pose tracking once the scale is estimated, so we can accumulate a period of observations,

waiting for an opportunity that the designed observability condition is satisfied.

The metric scale estimation problem in this paper is solved from the perspective of statistics and probability. As we know the direct observation from the region-based bundle adjustment is a compound motion of the object motion and camera motion, while the object motion and camera motion are supposed to be independent since they have no real physical connections. Thus the scale could be estimated based on the statistical independence of the object motion and camera motion in the world frame.

We start by analyzing the scale factor ( $s$ ) we want to estimate, it is actually a scale ratio of the real metric scale over the inherent scale exists in the region-based BA ( $\mathbf{p}_{o_t}^{c_t} = s \cdot \bar{\mathbf{p}}_{o_t}^{c_t}$ ). It is time-invariant if the region-based BA is accurate enough since it reflects the intrinsic scale of the tracked object. For the same reason, the intrinsic metric scale estimator needs not to perform for each input image. We call this scale ratio as scale in the following content for simplicity. Accordingly, the estimated scale  $\hat{s}$  could be represented as the sum of the true scale  $s$  and the estimation error  $\Delta s$ :

$$\hat{s} = s + \Delta s. \quad (3)$$

Recall the recovered object trajectory:

$$\hat{\mathbf{p}}_{o_t}^w = \hat{s} \cdot \mathbf{R}_{c_t}^w \bar{\mathbf{p}}_{o_t}^{c_t} + \mathbf{p}_{c_t}^w = \hat{s} \cdot \mathbf{p}_{d_t}^w + \mathbf{p}_{c_t}^w, \quad (4)$$

where

$$\mathbf{p}_{d_t}^w = \mathbf{R}_{c_t}^w \bar{\mathbf{p}}_{o_t}^{c_t}. \quad (5)$$

Particularly, when  $\hat{s}$  equals to  $s$ :

$$\mathbf{p}_{o_t}^w = s \cdot \mathbf{p}_{d_t}^w + \mathbf{p}_{c_t}^w. \quad (6)$$

Thus:

$$\begin{aligned} \hat{\mathbf{p}}_{o_t}^w &= \hat{s} \cdot \mathbf{p}_{d_t}^w + \mathbf{p}_{c_t}^w = (s + \Delta s) \cdot \mathbf{p}_{d_t}^w + \mathbf{p}_{c_t}^w \\ &= \mathbf{p}_{o_t}^w + \Delta s \cdot \mathbf{p}_{d_t}^w = \mathbf{p}_{o_t}^w + \frac{\Delta s}{s} (\mathbf{p}_{o_t}^w - \mathbf{p}_{c_t}^w) \\ &= (1 + \frac{\Delta s}{s}) \mathbf{p}_{o_t}^w - \frac{\Delta s}{s} \mathbf{p}_{c_t}^w, \end{aligned} \quad (7)$$

from the recovered object trajectory representation we can see that uncorrected scale estimation results in insufficient motion decomposition, which means the recovered object motion has some correlation with the camera motion. Thus the optimal scale could be estimated by correlation analysis between the recovered object motion and the corresponding camera motion. If the object motion and camera motion satisfies a certain observability condition within a time domain, we argue that an incorrect metric scale estimate, no matter larger or smaller than the true scale value, corresponds to a kind of salient correlation relationship between the recovered object motion and the camera motion. Thus a good scale estimate ( $\Delta s \rightarrow 0$ ) could be obtained by minimizing the correlation between the recovered object motion and the camera motion. Thus, the key objective function formulation is all about how to quantize the correlation properly.

We first model the recovered object motion and camera motion as two random variables  $\mathbf{m}_o$  and  $\mathbf{m}_c$ , and define another random variable  $\mathbf{m}_d$  to denote the up-to-scale motion

difference, here we adopt a certain order derivative of a motion trajectory for motion representation:

$$\begin{aligned} \mathbf{m}_c &= [m_c^x, m_c^y, m_c^z]^T = \frac{\partial^n \mathbf{p}_c^w(t)}{\partial t^n}, \\ \mathbf{m}_d &= [m_d^x, m_d^y, m_d^z]^T = \frac{\partial^n \mathbf{p}_d^w(t)}{\partial t^n}, \\ \hat{\mathbf{m}}_o &= \hat{\mathbf{m}}_o(\hat{s}) = [\hat{m}_o^x, \hat{m}_o^y, \hat{m}_o^z]^T = \frac{\partial^n \hat{\mathbf{p}}_o^w(t)}{\partial t^n} \\ &= \hat{s} \mathbf{m}_d + \mathbf{m}_c = (1 + \frac{\Delta s}{s}) \mathbf{m}_o - \frac{\Delta s}{s} \mathbf{m}_c. \end{aligned} \quad (8)$$

For example,  $n = 2$  corresponds to the acceleration, and we directly approximate the motions from the raw data:

$$\begin{aligned} \mathbf{m}_c &= \frac{\partial^2 \mathbf{p}_c^w(t)}{\partial t^2} \approx \frac{\mathbf{p}_{c_{t+2\Delta t}}^w - 2\mathbf{p}_{c_{t+\Delta t}}^w + \mathbf{p}_{c_t}^w}{\Delta t^2}, \\ \mathbf{m}_d &= \frac{\partial^2 \mathbf{p}_d^w(t)}{\partial t^2} \approx \frac{\mathbf{p}_{d_{t+2\Delta t}}^w - 2\mathbf{p}_{d_{t+\Delta t}}^w + \mathbf{p}_{d_t}^w}{\Delta t^2}. \end{aligned} \quad (9)$$

We will further design an observability condition later such that the quantitative correlation value between  $\hat{\mathbf{m}}_o$  and  $\mathbf{m}_c$  could be minimized for a good scale estimation  $\hat{s}$ . Take a look at this covariance matrix:

$$\begin{aligned} \text{Cov}(\hat{\mathbf{m}}_o, \mathbf{m}_c) &= E[(\hat{\mathbf{m}}_o - E[\hat{\mathbf{m}}_o])(\mathbf{m}_c - E[\mathbf{m}_c])^T] \\ &= E[(\hat{s} \mathbf{m}_d + \mathbf{m}_c - E[\hat{s} \mathbf{m}_d + \mathbf{m}_c])(\mathbf{m}_c - E[\mathbf{m}_c])^T] \\ &= \hat{s} \text{Cov}(\mathbf{m}_d, \mathbf{m}_c) + \text{Cov}(\mathbf{m}_c, \mathbf{m}_c). \end{aligned} \quad (10)$$

Particularly, when  $\hat{s}$  equals to  $s$ :

$$\text{Cov}(\mathbf{m}_o, \mathbf{m}_c) = s \text{Cov}(\mathbf{m}_d, \mathbf{m}_c) + \text{Cov}(\mathbf{m}_c, \mathbf{m}_c). \quad (11)$$

All the population covariances could be estimated from the latest  $N_o$  observations ( $N_o$  is a big enough but a limited number for bounded computation complexity consideration).

$$\begin{aligned} \text{Cov}(\mathbf{m}_d, \mathbf{m}_c) &\approx \frac{1}{N_o - 1} \sum_{k=1}^{N_o} (\mathbf{m}_d^k - \hat{\mathbf{m}}_d)(\mathbf{m}_c^k - \hat{\mathbf{m}}_c)^T, \\ \text{Cov}(\mathbf{m}_c, \mathbf{m}_c) &\approx \frac{1}{N_o - 1} \sum_{k=1}^{N_o} (\mathbf{m}_c^k - \hat{\mathbf{m}}_c)(\mathbf{m}_c^k - \hat{\mathbf{m}}_c)^T, \\ \hat{\mathbf{m}}_d &= \frac{1}{N_o} \sum_{k=1}^{N_o} \mathbf{m}_d^k, \quad \hat{\mathbf{m}}_c = \frac{1}{N_o} \sum_{k=1}^{N_o} \mathbf{m}_c^k. \end{aligned} \quad (12)$$

The standard correlation measurement between two multivariate random variables is to use trace correlation [20]. Instead, we utilize a simplified measurement in terms of individual covariances such that a closed form scale estimation could be derived. The objective function  $f(\hat{s})$  is formulated as the sum of all the covariance squares of Equation 10:

$$\begin{aligned} f(\hat{s}) &= \sum_{i,j \in x,y,z} \text{Cov}^2(\hat{m}_o^i, m_c^j) \\ &= \sum_{i,j \in x,y,z} (\hat{s} \text{Cov}(m_d^i, m_c^j) + \text{Cov}(m_c^i, m_c^j))^2 \\ &= \left( \sum_{i,j \in x,y,z} \text{Cov}^2(m_d^i, m_c^j) \right) \hat{s}^2 \\ &\quad + \left( \sum_{i,j \in x,y,z} 2\text{Cov}(m_d^i, m_c^j) \text{Cov}(m_c^i, m_c^j) \right) \hat{s} \\ &\quad + \sum_{i,j \in x,y,z} \text{Cov}^2(m_c^i, m_c^j), \end{aligned} \quad (13)$$

which is a quadratic function in terms of  $\hat{s}$ , thus the optimal scale estimation could be represented in a closed form solution through minimizing  $f(\hat{s})$ :

$$\hat{s}^* = - \frac{\sum_{i,j \in x,y,z} \text{Cov}(m_d^i, m_c^j) \text{Cov}(m_c^i, m_c^j)}{\sum_{i,j \in x,y,z} \text{Cov}^2(m_d^i, m_c^j)}. \quad (14)$$

### C. Observability condition derivation

One key point we want to highlight is that the scale estimator has degenerated cases using a monocular sensor scheme. In other words, our estimator will not work for all camera and object motion combinations. Take the case that the camera is almost static during the data accumulation for example, the optimal scale estimation result  $\hat{s}$  will be tending to zero, which is definitely not correct. This is because the observed compound object motion in the camera frame that combines object motion and camera motion degenerates to object motion only, and the constraint derived from the motion decomposition process doesn't hold anymore.

In addition, note that all the computation is based on the motion independence assumption, thus another possible degenerated case is that the camera moves exactly as how the object moves, resulting in an invariable observation of the object in the camera frame. Although this case is statistically of very low probability, the corresponding optimal scale value  $\hat{s}$  can be arbitrary numbers. On the other hand, however, it is also almost impossible that the object motion and the camera motion are strictly uncorrelated in a limited sample duration time. Thus an error term  $\Delta s$  exists in practical analysis within a specific observation duration. Nevertheless, the estimation is still valid if the error term is limited to an acceptable range, and we call the corresponding condition as the observability condition. And our intrinsic scale estimator do not have to be running all the time since what we estimate is the intrinsic scale of the tracked object instead of object depths of the input sequential images. Estimating the intrinsic scale once in a while when the observability condition is satisfied is totally acceptable because of the region-based BA in our system.

In fact, the observability condition is more important than the closed form scale estimation to some extent, since it determines if we can accept the scale estimation or not. One intuitive condition is that the objective function value with the optimal scale should be close to zero, but intuitive way may miss some degenerated cases, so a better way is to study the observability condition through error term analysis (substitute Equation 3 and 11 into Equation 14):

$$\frac{\Delta s^*}{s} = \frac{\sum_{i,j \in x,y,z} \text{Cov}(m_o^i, m_c^j) (\text{Cov}(m_c^i, m_c^j) - \text{Cov}(m_o^i, m_c^j))}{\sum_{i,j \in x,y,z} (\text{Cov}(m_c^i, m_c^j) - \text{Cov}(m_o^i, m_c^j))^2}. \quad (15)$$

The desired scale estimation should satisfy  $\frac{\Delta s^*}{s} \rightarrow 0$ , and we summarize it as:

$$\begin{aligned} \sum_{i,j \in x,y,z} \text{Cov}^2(m_o^i, m_c^j) &\rightarrow 0, \\ \frac{1}{\sum_{i,j \in x,y,z} \text{Cov}^2(m_c^i, m_c^j)} &\rightarrow 0, \end{aligned} \quad (16)$$

where the first condition just meets the intuitive condition if we use the reconstructed object motion with the optimal scale ( $\hat{\mathbf{m}}_o(\hat{s}^*)$ ) instead of the real object motion ( $\mathbf{m}_o$ ), so it's a necessary condition. The second condition is totally under control on the other hand, since although we cannot control the camera motion, but we can at least observe and analyze the camera motion to decide if the scale estimation is acceptable or not.

In practice, we use the threshold-based criteria instead:

$$\begin{aligned} \sum_{i,j \in x,y,z} \text{Cov}^2(m_o^i, m_c^j) &\leq \epsilon_{t_1}, \\ \sum_{i,j \in x,y,z} \text{Cov}^2(m_c^i, m_c^j) &\geq \rho_{t_1}. \end{aligned} \quad (17)$$

Also, for the numerical stability of Equation 14:

$$\sum_{i,j \in x,y,z} \text{Cov}^2(m_d^i, m_c^j) \geq \rho_{t_2}. \quad (18)$$

So far, we can derive the complete observability condition as follows:

$$\begin{aligned} \text{i} \quad & f(\hat{s}^*) \leq \epsilon_{t_1} \\ \text{ii} \quad & \sum_{i,j \in x,y,z} \text{Cov}^2(m_c^i, m_c^j) \geq \rho_{t_1} \\ \text{iii} \quad & \sum_{i,j \in x,y,z} \text{Cov}^2(m_d^i, m_c^j) \geq \rho_{t_2}, \end{aligned} \quad (19)$$

where  $\epsilon_{t_1}$  is a threshold with small positive value,  $\rho_{t_1}$  and  $\rho_{t_2}$  are two thresholds with large enough positive values. The first two subconditions are used to satisfy the estimation accuracy requirement, and the last subcondition is for numerical stability consideration. All the thresholds are set empirically in implementation. The more strict the condition is, the more accurate and robust the metric scale estimator will be, but with lower scale acceptance rate. Overall, the observability condition makes our system robust against multiple degenerated cases that may occur in the tracking process.

Given the estimated metric scale with the observability condition satisfied, we can first recover the object position in the camera frame as:

$$\hat{\mathbf{p}}_{O_t}^{c_t} = \hat{s} \cdot \hat{\mathbf{p}}_{O_t}^{c_t}, \quad (20)$$

then we can recover the object poses in the world frame:

$$\begin{aligned} \hat{\mathbf{R}}_{O_t}^w &= \hat{\mathbf{R}}_{c_t}^w \hat{\mathbf{R}}_{O_t}^{c_t}, \\ \hat{\mathbf{p}}_{O_t}^w &= \hat{s} \cdot \hat{\mathbf{R}}_{c_t}^w \hat{\mathbf{p}}_{O_t}^{c_t} + \hat{\mathbf{p}}_{c_t}^w. \end{aligned} \quad (21)$$

It is evident that the final object localization performance relies on VINS ( $\hat{\mathbf{p}}_{c_t}^w$  and  $\hat{\mathbf{R}}_{c_t}^w$ ), up-to-scale 3D tracking ( $\hat{\mathbf{p}}_{O_t}^{c_t}$  and  $\hat{\mathbf{R}}_{O_t}^{c_t}$ ) and metric scale estimation results ( $\hat{s}$ ).

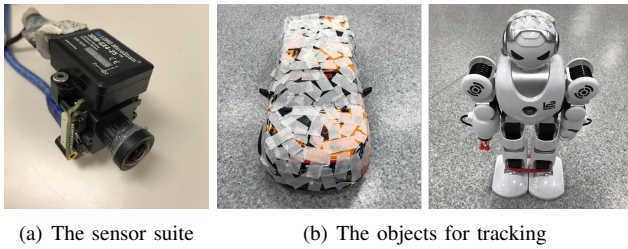


Fig. 6: The minimal sensor suite and irregular objects we use for experiments. Our method do not need any prior knowledge, special markers or tags of the tracking object.

## V. EXPERIMENTAL RESULTS

### A. Implementation details

Our monocular sensor suite (Fig. 6(a)) consists of an mvBlueFOX-MLC202bG grayscale camera with a wide-angle lens that captures 1280 by 960 images at 24 Hz and a Microstrain 3DM-GX4 IMU that runs at 500 Hz. Both VINS and 2D tracker work on the downsampled images of 640 by 480 resolution. We use CMT tracker [18] as the 2D tracker in our implementation and manually draw the object area for 2D tracking initialization. While the cropped images according to 2D tracking results are used for region-based bundle adjustment ( $N = 20$  in sliding window). For robust region-based BA estimation, the object area extracted from the original image cannot be too small, which means the object cannot be too far away from the camera. In practice, we notice that at least 50 features should be extracted from the object region if we use feature-based tracking frontend. The number of observations we use for metric scale estimation is 200 ( $N_o = 200$ ). The motion feature extracted is velocity ( $n = 1$  in Equation 8). The whole system runs on a desktop computer in real time.

The goal of the experiments is to validate the recovered object pose in the world frame ( $\mathbf{R}_o^w$  and  $\mathbf{p}_o^w$ ) by involving the camera pose in the world frame and the estimated metric scale. Since there are no similar formulations shown in relevant works, we evaluate our estimation accuracy with a comparison to a motion capture system (OptiTrack) as groundtruth. And we use several general objects as the tracking targets. Two sample objects are shown in Fig. 6(b), where the tapes attached on the objects are used to cover the excessively shining parts that may deactivate the motion capture system.

### B. 6-DoF dynamic object pose estimation in world frame

Given the estimated metric scale, the 3D tracking results could be projected to the world frame using Equation 21. For trial 1, a manually controlled toy robot is adopted as the tracking target. While for trial 2, a remote controlled racing car is used as the tracking target, which is controlled to run from ground to a higher platform with directions changing all the time. More details and AR demonstration will be shown in the attached video.

Fig. 7 and Fig. 8 show part of the position and orientation comparison between the estimation and groundtruth,

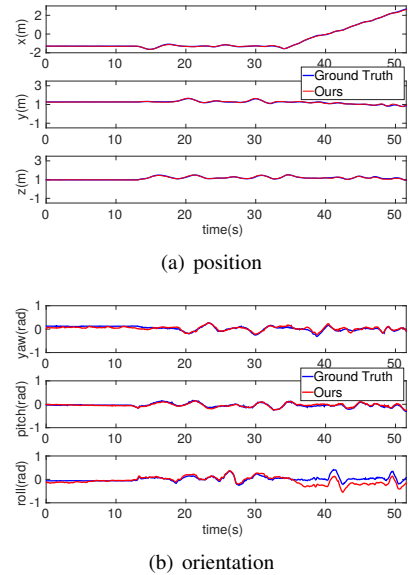


Fig. 7: The comparison of 6-DoF object pose estimation (Trial 1: tracking a manually controlled toy robot).

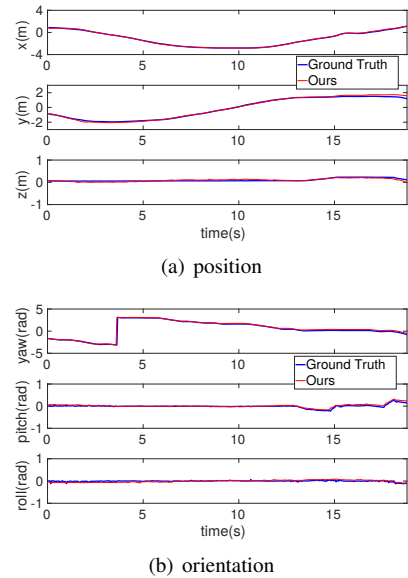


Fig. 8: The comparison of 6-DoF object pose estimation (Trial 2: tracking a remote controlled racing car).

with a standard deviation of  $\{0.0486, 0.0271, 0.1245\}$  (rad) in yaw, pitch and roll, a standard deviation of  $\{0.0218, 0.0310, 0.0344\}$  (m) in the  $x$ ,  $y$  and  $z$  positions of trial 1, and a standard deviation of  $\{0.0739, 0.0254, 0.0239\}$  (rad) in yaw, pitch and roll, a standard deviation of  $\{0.0505, 0.1169, 0.0397\}$  (m) in the  $x$ ,  $y$  and  $z$  positions of trial 2. Generally, the experiment shows acceptable performance of our 6-DoF object tracking system. We can also notice the orientation drift of trial 1 and translation drift of trial 2 caused by the up-to-scale 3D tracker module, which could be corrected by visual relocalization or loop closure if a loop is detected.

TABLE I: Degenerated cases

Cases	true scale $s$	sample estimations $\hat{s}$	observability subcondition
$C_1$	0.43	(-5.99 -4.62 -2.71 -1.13 16.87 35.85 12.27 17.19 -0.38 -0.26)	(i) not satisfied
$C_2$	0.43	(0.047 -0.008 -0.039 -0.041 -0.007 -0.031 -0.067 0.017 0.008 0.009)	(ii) not satisfied
$C_3$	0.43	(-0.085 -0.088 -0.0085 -0.078 -0.077 -0.085 -0.078 -0.085 -0.078 -0.076)	(ii) not satisfied
$C_4$	0.43	(21.81 20.82 19.76 18.82 27.38 25.14 21.57 22.77 21.57 24.15)	(iii) not satisfied

### C. Degenerated cases

We further test three typical degenerated cases that will generate inaccurate scale estimation without checking the observability condition: the camera moves exactly as how the car moves in terms of translation ( $C_1$ ); the camera is inactive, static ( $C_2$ ), constant velocity ( $C_3$ ); and static object observation in the camera frame although both the car and the camera are moving ( $C_4$ ), which correspond to the three observability subconditions discussed in Equation 19 respectively. And all these degenerated cases could be avoided by checking the observability condition. The true scale, sample scale estimations under these cases, and corresponding subconditions are listed in Table I. According to Equation 15, the scale estimations may have large estimation errors for case  $C_1$  ( $\text{Cov}(m_o^i, m_c^j) \rightarrow 0$ ). According to Equation 14, the scale estimations tend to be approaching to zero for case  $C_2$  and case  $C_3$  ( $\text{Cov}(m_c^i, m_c^j) \rightarrow 0$ ). And according to Equation 14, the scale estimations tend to have large absolute values for case  $C_4$  ( $\text{Cov}(m_d^i, m_c^j) \rightarrow 0$ ). Fortunately, all the degenerated cases could be avoided by checking the observability condition during the tracking process.

## VI. CONCLUSION AND FUTURE WORK

In this paper, we propose a new understanding of the 6-DoF object tracking problem using a monocular sensor suite with visual-inertial fusion. We have proven the feasibility of the proposed 3D tracking system with observability condition analysis. The experimental results validate our idea and show an acceptable estimation accuracy of the proposed method. At the same time, each module in our system has upgrading potential. For example, the region-based bundle adjustment implemented in this paper is purely a BA without relocalization, loop-closure which are widely used in the visual odometry community. Thanks to the building block design of our system, fortunately, each module can be conveniently replaced, and the whole system will be boosted accordingly.

### REFERENCES

- [1] Y. Lin, F. Gao, T. Qin, W. Gao, T. Liu, W. Wu, Z. Yang, and S. Shen, "Autonomous aerial navigation using monocular visual-inertial fusion," *Journal of Field Robotics*, 2017.
- [2] Z. Yang, F. Gao, and S. Shen, "Real-time monocular dense mapping on aerial robots using visual-inertial fusion," in *Robotics and Automation (ICRA), 2017 IEEE International Conference on*. IEEE, 2017, pp. 4552–4559.
- [3] A. Aldoma, F. Tombari, J. Prankl, A. Richtsfeld, L. Di Stefano, and M. Vincze, "Multimodal cue integration through hypotheses verification for rgb-d object recognition and 6dof pose estimation," in *Robotics and Automation (ICRA), 2013 IEEE International Conference on*. IEEE, 2013, pp. 2104–2111.
- [4] M.-S. Wang *et al.*, "3d object pose estimation using stereo vision for object manipulation system," in *Applied System Innovation (ICASI), 2017 International Conference on*. IEEE, 2017, pp. 1532–1535.
- [5] A. Rozantsev, S. N. Sinha, D. Dey, and P. Fua, "Flight dynamics-based recovery of a uav trajectory using ground cameras," *arXiv preprint arXiv:1612.00192*, 2016.
- [6] M. Vo, S. G. Narasimhan, and Y. Sheikh, "Spatiotemporal bundle adjustment for dynamic 3d reconstruction," in *Proceedings of the IEEE Conference on Computer Vision and Pattern Recognition*, 2016, pp. 1710–1718.
- [7] S. Garrido-Jurado, R. Muñoz-Salinas, F. J. Madrid-Cuevas, and M. J. Marín-Jiménez, "Automatic generation and detection of highly reliable fiducial markers under occlusion," *Pattern Recognition*, vol. 47, no. 6, pp. 2280–2292, 2014.
- [8] K. Qiu, T. Liu, and S. Shen, "Model-based global localization for aerial robots using edge alignment," *IEEE Robotics and Automation Letters*, vol. 2, no. 3, pp. 1256–1263, 2017.
- [9] K. Qiu and S. Shen, "Model-aided monocular visual-inertial state estimation and dense mapping," in *Intelligent Robots and Systems (IROS), 2017 IEEE/RSJ International Conference on*. IEEE, 2017, pp. 1783–1789.
- [10] S. Garrido-Jurado, R. M. noz Salinas, F. Madrid-Cuevas, and M. Marín-Jiménez, "Automatic generation and detection of highly reliable fiducial markers under occlusion," *Pattern Recognition*, vol. 47, no. 6, pp. 2280 – 2292, 2014.
- [11] S. Leutenegger, M. Chli, and R. Y. Siegwart, "Brisk: Binary robust invariant scalable keypoints," in *Computer Vision (ICCV), 2011 IEEE International Conference on*. IEEE, 2011, pp. 2548–2555.
- [12] E. Brachmann, F. Michel, A. Krull, M. Ying Yang, S. Gumhold *et al.*, "Uncertainty-driven 6d pose estimation of objects and scenes from a single rgb image," in *Proceedings of the IEEE Conference on Computer Vision and Pattern Recognition*, 2016, pp. 3364–3372.
- [13] C. Choi and H. I. Christensen, "3d textureless object detection and tracking: An edge-based approach," in *Intelligent Robots and Systems (IROS), 2012 IEEE/RSJ International Conference on*. IEEE, 2012, pp. 3877–3884.
- [14] A. Zeng, K.-T. Yu, S. Song, D. Suo, E. Walker, A. Rodriguez, and J. Xiao, "Multi-view self-supervised deep learning for 6d pose estimation in the amazon picking challenge," in *Robotics and Automation (ICRA), 2017 IEEE International Conference on*. IEEE, 2017, pp. 1386–1383.
- [15] G. Pavlakos, X. Zhou, A. Chan, K. G. Derpanis, and K. Daniilidis, "6-dof object pose from semantic keypoints," *arXiv preprint arXiv:1703.04670*, 2017.
- [16] Z. Yang and S. Shen, "Monocular visual-inertial state estimation with online initialization and camera-imu extrinsic calibration," *IEEE Transactions on Automation Science and Engineering*, no. 99, p. 1, 2016.
- [17] T. Qin and S. Shen, "Robust initialization of monocular visual-inertial estimation on aerial robots," in *Proc. of the IEEE/RSJ Intl. Conf. on Intell. Robots and Syst.*, Vancouver, Canada, 2017, accepted.
- [18] G. Nebelbay and R. Pflugfelder, "Clustering of static-adaptive correspondences for deformable object tracking," in *Proceedings of the IEEE Conference on Computer Vision and Pattern Recognition*, 2015, pp. 2784–2791.
- [19] S. Hare, S. Golodetz, A. Saffari, V. Vineet, M.-M. Cheng, S. L. Hicks, and P. H. Torr, "Struck: Structured output tracking with kernels," *IEEE transactions on pattern analysis and machine intelligence*, vol. 38, no. 10, pp. 2096–2109, 2016.
- [20] J. W. Hooper, "Simultaneous equations and canonical correlation theory," *Econometrica: Journal of the Econometric Society*, pp. 245–256, 1959.